Congreso de Métodos Numéricos en Ingeniería 2009
Barcelona, 29 junio al 2 de julio 2009

MODELLING FRC INFRASTRUCTURES TAKING INTO ACCOUNT THE SOIL-STRUCTURE INTERACTION

Joaquim A. O. Barros[1], Marco di Prisco[2], Cláudio di Prisco[2]

1: ISISE – Institute for Sustainability and Innovation in Structural Engineering
Department of Civil Engineering
University of Minho
Campus de Azurém, Guimarães, Portugal
e-mail: barros@civil.uminho.pt, web: http://www.isise.net

2: Department of Structural Engineering, Polytechnic of Milan
Piazza Leonardo da Vinci, 32, 20133 Milano, Italy
e-mail: {mdiprisc,cdiprisc}@stru.polimi.it, Web: http://www.polimi.it

Keywords: Fibre reinforced concrete, box-culvert, finite element method, material nonlinear analysis

Abstract. *The favourable effect that fibres provide at concrete crack initiation and propagation is especially notable in structures of high redundant supports, such is the case of concrete infrastructures surrounded by soil. If the design of these concrete structures is governed by crack width restrictions, fibre reinforced concrete is even a more competitive solution, since the stress redistribution provided by fibres bridging the micro-cracks allows the formation of diffuse crack patterns of reduced crack width. If these structures are precast with high strength concrete, and composed by thin walled components, fibres can effectively replace the total conventional transversal reinforcement, as well as a significant percentage of flexural reinforcement, resulting high competitive structures in economic and functional terms. However, to assess the fibre reinforcement benefits in this type of engineering problems, the concrete post-cracking behaviour and the soil-structure interaction behaviour need to be modelled as accurately as possible. In this paper, a FEM-based model is briefly developed and applied to box-culvert structures. The model is described and a preliminary application is analysed. The main results are presented and discussed.*

1. INTRODUCTION

The crack opening arrestment provided by the reinforcement mechanisms of fibres bridging the crack surfaces of cement based materials lead to significant increase in terms of load carrying capacity and energy dissipation capability of concrete structures, mainly those of high redundant support conditions, such is the case of structures surrounded by

soil. In fact, as higher is the degree of static indeterminacy, as competitive can be the replacement of conventional steel bars by discrete steel fibres, since stress redistribution provided by fibre reinforcement allows an ultimate load much higher than the cracking load. In several underground reinforced concrete (RC) structures, crack width limit is the governing design condition, since a crack width higher than a certain value can compromise the durability and the functionality of theses structures, with economic and technical harmful consequences.

Box-culvert is one of this type of underground concrete structures, formed by a bottom and a top U shape RC laminar elements connected by a concrete-concrete hinge connection (Fig. 1). Box-culverts are used for several purposes, like underground passages for persons, vehicles or animals (Fig. 1). These RC structures are subject to the soil dead weight, which in certain cases can attain a cover layer 20m thick. Other constructions can also transfer loads to the box-culverts. On the soil surface, a live load (LL) can also actuate due to the action of vehicles or other non-permanent loads.

Fig. 1 – Examples of application of box-culvert.

Since the construction of this infra-structure is made by phases, the numerical simulation of this construction process is mandatory for a realistic prediction of the behaviour of the intervening materials and structures. Fig. 2 represents the current construction phase process used in this type of infra-structure. In general, the construction process is composed of 6 phases. In this figure [P_i-P_j] means a material or structural component pertaining to phases P_i up to P_j.

Fig. 3a represents the reinforcement detailing for the box-culvert, whose geometry of the top part is shown in Fig. 3b. According to the information provided by a precast company, this reinforcement (118.5 kg/m^3) was designed for an embankment soil layer thickness (H_{ST}) of 4 m (Fig. 2). In the present work the use of a self compacting concrete reinforced with 45 kg/m^3 of hooked ends steel fibres (SFRSCC), developed within the ambit of an applied research project [1], was explored with the purpose of verifying the possibility of replacing the reinforcement applied in the box-culvert of Fig. 3. In this example H_{sB}=3.64m, H_{sT}=4.0m and the width of the trench is 9.1m.

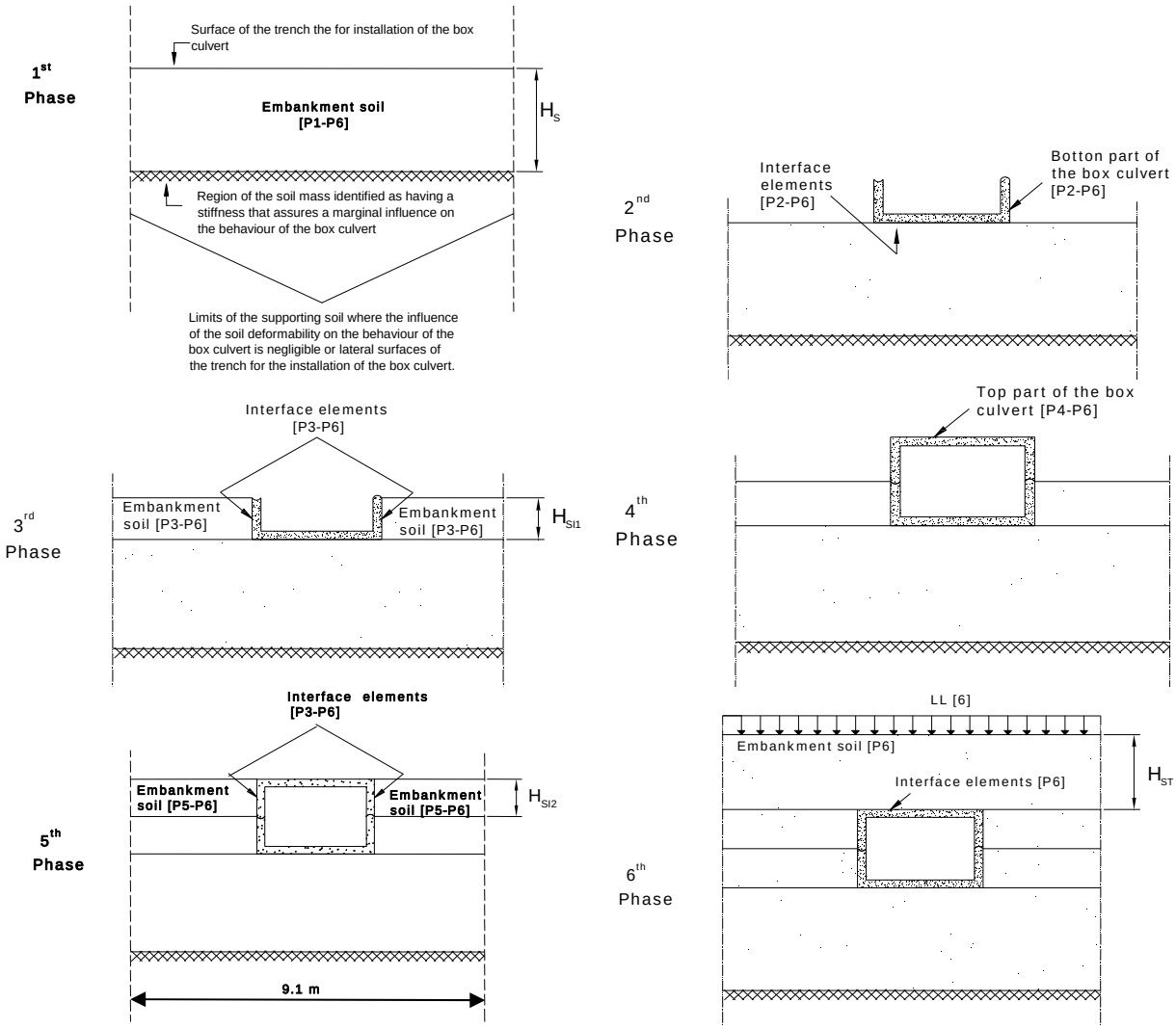

Figure 2 – Phase construction process.

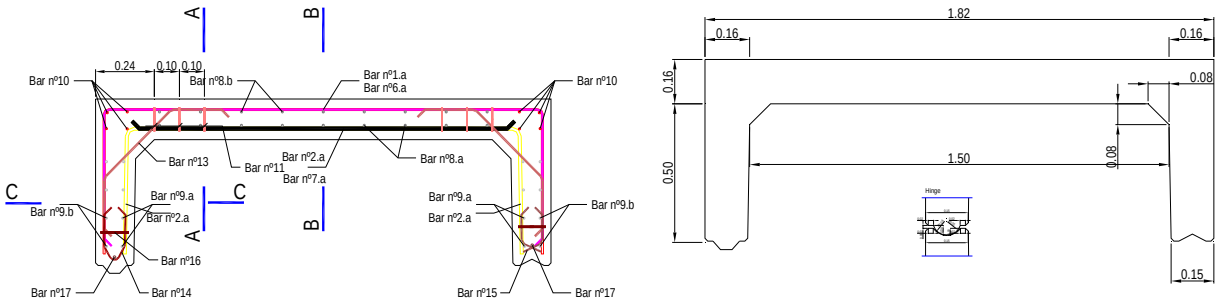

Fig. 3 – (a) Geometry and (b) reinforcement (dimensions in m).

Furthermore, the live load (LL of Fig. 2) that can be applied up to introduce a maximum crack width of 0.3 mm in the box-culvert will be evaluated, since below to this crack

width the durability performance of SFRSCC is not affected by the action of the aggressiveness of environmental agents.

2. NUMERICAL MODEL

2.1. Software for nonlinear material analysis

The new numerical facilities were introduced into FEMIX 4.0, which is a computer code whose purpose is the analysis of structures by the Finite Element Method (FEM) [2]. The first Author is a co-founder of FEMIX. This code is based on the displacement method, being a large library of types of finite elements already available. All these types of elements can be simultaneously included in the same analysis, with the exception of some incompatible combinations. The analysis may be static or dynamic and the material behavior may be linear or nonlinear. Data input is facilitated by the possibility of importing CAD models. Post processing is performed with a general purpose scientific visualization program named *drawmesh*. In the same nonlinear analysis several nonlinear models may be simultaneously considered. Interface elements with appropriate friction laws and nonlinear springs may also be simultaneously considered. The global response history is recorded in all the sampling points for selected post-processing. Advanced numerical techniques are available, such as the Newton-Raphson method combined with arc-length techniques and path dependent or independent algorithms. When the size of the systems of linear equations is very large, a preconditioned conjugate gradient method can be advantageously used.
For the analysis of FRC infrastructures taking into account the soil-structure interaction, the first Author implemented the following new facilities into FEMIX: i) the simulation of phasing construction; ii) constitutive models for soil, one based on the elasto-plasticity Mohr-Coulomb criterion and the other on the Ottosen failure criterion; the smeared crack model to simulate the crack initiation and propagation in box-culvert, already existing for plane stress state problems, was adapted for modelling the behaviour of structures considered in plane strain state conditions, such is the case of the present study; iii) opening-sliding constitutive model for interface finite elements to simulate the soil-concrete interaction. The main characteristics of these constitutive models are described in next sections.

2.2. Constitutive model for the FRC

The concrete cracking is simulated under the framework of the multifixed smeared crack concepts [3]. According to the present model, the total strain increment of the cracked concrete, $\Delta\underline{\varepsilon}$, is the addition of the strain increment in the fracture zone, $\Delta\underline{\varepsilon}^{cr}$, with the strain increment of the concrete between cracks, $\Delta\underline{\varepsilon}_e^{co}$:

$$\Delta\underline{\varepsilon} = \Delta\underline{\varepsilon}_e^{co} + \Delta\underline{\varepsilon}^{cr} \quad (1)$$

For the present study, concrete between cracks is assumed in elastic (*e*) behaviour, but elasto-plastic behaviour can also be simulated [4]. The concrete is governed by the following constitutive equation:

$$\Delta\underline{\sigma}=\underline{D}^{co}\Delta\underline{\varepsilon}^{co} \tag{2}$$

where, in the case of uncracked linear-elastic material, $\underline{D}^{co}$ becomes with the designation of $\underline{D}_e^{co}$, with the following format:

$$\underline{D}^{co} \rightarrow \underline{D}_e^{co} = \frac{E_c}{\left(1+\upsilon_c\right)\left(1-2\,\upsilon_c\right)}\begin{bmatrix} \left(1-\upsilon_c\right) & \upsilon_c & 0 \\ \upsilon_c & \left(1-\upsilon_c\right) & 0 \\ 0 & 0 & \dfrac{1-2\,\upsilon_c}{2} \end{bmatrix} \tag{3}$$

where υ_c and E_c are the Poisson coefficient and the Young's modulus of the uncracked concrete, respectively. In the present study, the structure is considered in the *yz* plane and the stress component orthogonal to the structure, σ_x, is not considered in the present crack constitutive model, i.e., it is assumed that cracks do not form in parallel to the plane of the structure. When cracked, $\underline{D}^{co}$ has the following configuration [5]:

$$\underline{D}^{co} \rightarrow \underline{D}_{ecr}^{co} = \left\{\underline{D}_e^{co} - \underline{D}_e^{co}\,\underline{T}^{crT}\left[\underline{D}^{cr} + \underline{T}^{cr}\,\underline{D}_e^{co}\,\underline{T}^{crT}\right]^{-1}\underline{T}^{cr}\,\underline{D}_e^{co}\right\} \tag{4}$$

where $\underline{T}^{cr}$ is a matrix defining the orientation of the cracks formed at a sampling point. If *m* cracks occurs at a sampling point:

$$\underline{T}^{cr} = \left[\underline{T}_1^{cr} \quad , \quad \underline{T}_i^{cr} \quad , \quad \underline{T}_m^{cr}\right]^T \tag{5}$$

where the crack orientation of a generic i^{th} crack is defined by the matrix $\underline{T}_i^{cr}$:

$$\underline{T}_i^{cr} = \begin{bmatrix} \cos^2\theta_i & \sin^2\theta_i & 2\sin\theta_i\cos\theta_i \\ -\sin\theta_i\cos\theta_i & \sin\theta_i\cos\theta_i & \cos^2\theta_i-\sin^2\theta_i \end{bmatrix} \tag{6}$$

with θ_i being the angle between *y* and the normal to the i^{th} crack plane (see Fig. 4). In (4) $\underline{D}^{cr}$ is a matrix including the constitutive law of the cracks:

$$\underline{D}^{cr} = \begin{bmatrix} \underline{D}_1^{cr} & \dots & \underline{0} & \dots & \underline{0} \\ \dots & \dots & \dots & \dots & \dots \\ \underline{0} & \dots & \underline{D}_i^{cr} & \dots & \underline{0} \\ \dots & \dots & \dots & \dots & \dots \\ \underline{0} & \dots & \underline{0} & \dots & \underline{D}_m^{cr} \end{bmatrix} \tag{7}$$

where $\underline{D}_i^{cr}$ is the i^{th} crack constitutive law:

$$\underline{D}_i^{cr} = \begin{bmatrix} D_{I,i}^{cr} & 0 \\ 0 & D_{II,i}^{cr} \end{bmatrix} \tag{8}$$

with D_I^{cr} and D_{II}^{cr} being the crack fracture mode I and mode II stiffness modulus, respectively. The crack system of a sampling point is governed by the following relationship:

$$\Delta\underline{\sigma}^{cr} = \underline{D}^{cr}\,\Delta\underline{\varepsilon}^{cr} \tag{9}$$

where $\Delta\underline{\sigma}^{cr}$ is the vector of the incremental crack stress components (Fig. 4):

$$\Delta\underline{\sigma}^{cr} = \begin{bmatrix} \Delta\sigma_{n,1}^{cr} & \Delta\tau_{nt,1}^{cr} & \dots & \Delta\sigma_{n,i}^{cr} & \Delta\tau_{nt,i}^{cr} & \dots & \Delta\sigma_{n,m}^{cr} & \Delta\tau_{nt,m}^{cr} \end{bmatrix}^T \tag{10}$$

and $\Delta\underline{\varepsilon}^{cr}$ is the vector of the incremental crack strain components:

$$\Delta\underline{\varepsilon}^{cr} = \begin{bmatrix} \Delta\varepsilon_{n,1}^{cr} & \Delta\gamma_{nt,1}^{cr} & \dots & \Delta\varepsilon_{n,i}^{cr} & \Delta\gamma_{nt,i}^{cr} & \dots & \Delta\varepsilon_{n,m}^{cr} & \Delta\gamma_{nt,m}^{cr} \end{bmatrix}^T \tag{11}$$

The D_I^{cr} of (8) is characterised by the fracture parameters (Fig. 5), namely, the tensile strength, $\sigma_{n,1}^{cr} = f_{ct}$, the fracture energy, G_f, the shape of the softening law and the crack bandwidth, l_b. Fibre reinforcement mechanisms are reflected, mainly, on the energy dissipated in the mode I fracturing process and on the shape of the softening branch. For fibre contents used in current concrete applications, the remaining concrete properties are only marginally affected by fibre addition [6]. The crack mode I stiffness is simulated by the trilinear diagram represented in Fig. 5.

The fracture mode II modulus, D_{II}^{cr}, is obtained from the equation [3, 6]:

$$D_{II}^{cr} = \frac{\beta}{1-\beta} G_c \tag{12}$$

where G_c is the concrete shear modulus and,

$$\beta = \left[1 - \frac{\varepsilon_n^{cr}}{\varepsilon_{n,u}^{cr}} \right]^p \quad \text{(p=1, 2 or 3)} \tag{13}$$

is the shear retention factor.

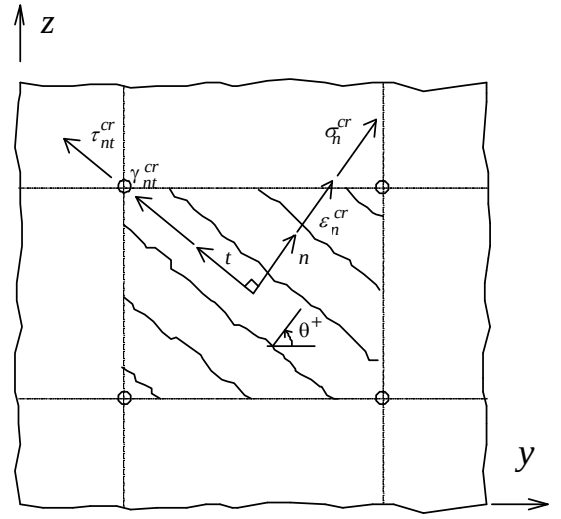

Fig. 4 - Crack stress and crack strain components.

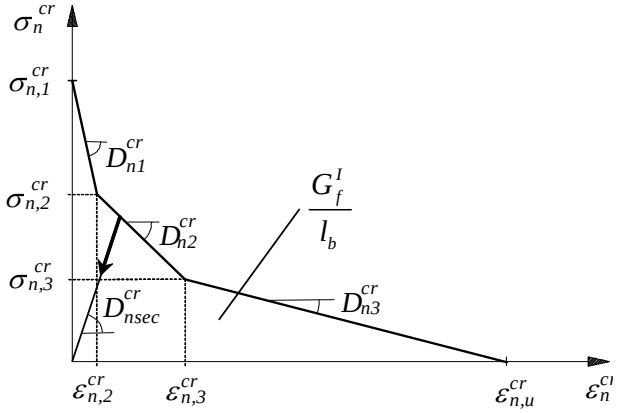

Fig. 5 - Stress-strain diagram for modelling the crack opening process.

Based on previous research on the development of SFRSCC for laminar structures [1], the values for the properties indicated in Table 1 were taken for the simulation of the box-culvert, assuming this structure will be precast with this material, in order to verify the possibility of replacing the conventional reinforcement used in the type of box-culvert in analysis in the present study. The values of the fracture parameters were obtained from inverse analysis [7]. In the numerical simulation, l_b was considered equal to the square root of the area of the finite element, a maximum of two cracks per sampling point can be formed, the threshold angle for the control of opening a new crack in a sampling point was considered equal to 30 degrees, and p=3 was taken for the evaluation of the shear retention factor, in eq. (13).

γ_c (kN/m^3)	E_c (GPa)	υ_c (-)	f_c (MPa)	$f_{ct} = \sigma_{n,I}^{cr}$ (MPa)	G_f (N/mm)	$\varepsilon_{n,2}^{cr} / \varepsilon_{n,u}^{cr}$	$\sigma_{n,2}^{cr} / \sigma_{n,1}^{cr}$	$\varepsilon_{n,3}^{cr} / \varepsilon_{n,u}^{cr}$	$\sigma_{n,3}^{cr} / \sigma_{n,1}^{cr}$
24.0	39.0	0.2	45.0	2.90	4.0	0.05	0.60	0.20	0.20

Table 1 – Values of the properties for the SFRSCC crack constitutive model.

2.3. Constitutive model for the soil

To simulate the behaviour of the embankment soil, the Mohr-Coulomb yield criterion is used:

$$f\left(\underline{\sigma},c,\phi\right)=\frac{1}{3}I_1\sin\phi+J_2^{1/2}\left(\cos\theta-\frac{1}{\sqrt{3}}\sin\theta\sin\phi\right)-c\cos\phi \tag{14}$$

where c and ϕ are the soil cohesion and the friction angle, I_1 and J_2 are the first invariant and the second deviatoric stress invariant, respectively, [8], and

$$\theta=\frac{1}{3}\arcsin\left(-\frac{3\sqrt{3}}{2}\frac{J_3}{J_2^{3/2}}\right) \tag{15}$$

with J_3 being the third deviatoric stress invariant [8].
For a plane strain problem, the stress vector has four components:

$$\underline{\sigma}=\left\{\sigma_x\quad\sigma_y\quad\sigma_z\quad\tau_{yz}\right\} \tag{16}$$

According to the plasticity theory principles, the flux vector $\underline{a}$ is composed by the four derivatives of the yield function with respect to each of the four stress components:

$$\underline{a}=\left\{\frac{\partial f\left(\underline{\sigma}\right)}{\partial\sigma_x}\quad\frac{\partial f\left(\underline{\sigma}\right)}{\partial\sigma_y}\quad\frac{\partial f\left(\underline{\sigma}\right)}{\partial\sigma_z}\quad\frac{\partial f\left(\underline{\sigma}\right)}{\partial\tau_{yz}}\right\} \tag{17}$$

The equation that defines each of the four flux vector $\underline{a}$ components is, in indicial notation, the following:

$$\begin{aligned}a_i&=\frac{\partial f\left(\underline{\sigma}\right)}{\partial\sigma_i}\\&=\frac{1}{3}\sin\phi\frac{\partial I_1}{\partial\sigma_i}+\frac{1}{2}\frac{\partial J_2}{\partial\sigma_i}J_2^{-1/2}\left(\cos\theta-\frac{1}{\sqrt{3}}\sin\theta\sin\phi\right)+\\&\frac{\sqrt{3}}{2}\frac{\frac{\partial J_3}{\partial\sigma_i}J_2-\frac{3}{2}\frac{\partial J_2}{\partial\sigma_i}J_3}{J_2^2\sqrt{1-\left(\sin3\theta\right)^2}}\left(\sin\theta+\frac{1}{\sqrt{3}}\cos\theta\sin\phi\right)\end{aligned} \tag{18}$$

To avoid the singularities at $\theta=\pm30^\circ$ the a_i takes the following form:

$$a_i=\frac{1}{3}\sin\phi\frac{\partial I_1}{\partial\sigma_i}+\frac{1}{2}\frac{\partial J_2}{\partial\sigma_i}J_2^{-1/2}\left(\frac{\sqrt{3}}{2}\pm\frac{1}{2\sqrt{3}}\sin\phi\right)\quad(\text{- for }\theta=30^\circ\text{ and + for }\theta=-30^\circ) \tag{19}$$

The derivatives of the invariants can be found in any book of elasto-plasticity theory [8].

To accomplish the Mohr-Coulomb yield surface, the return-mapping algorithm was implemented [9], having been obtained the following two equations system (for the generic *k* iteration of a load step *n*+1):

$$\begin{bmatrix} \underline{D}_s^{-1} + \Delta\lambda_{n+1}^k \dfrac{\partial^2 f_{n+1}^k}{\partial\left(\underline{\sigma}_{n+1}^k\right)^2} & \dfrac{\partial f_{n+1}^k}{\partial \underline{\sigma}_{n+1}^k} \\ \dfrac{\partial f_{n+1}^k}{\partial \underline{\sigma}_{n+1}^k} & 0 \end{bmatrix} \begin{bmatrix} d\underline{\sigma}_{n+1}^k \\ d\lambda_{n+1}^k \end{bmatrix} = -\begin{bmatrix} r_{\underline{\varepsilon}_{n+1}}^k \\ r_{f_{n+1}}^k \end{bmatrix} \tag{20}$$

that is solved by the Newton-Raphson numerical technique, where

$$\left(\Delta\underline{\varepsilon}_{n+1}^p\right)^k = \Delta\lambda_{n+1}^k \frac{\partial f_{n+1}^k}{\partial \underline{\sigma}_{n+1}^k} \tag{21}$$

is the strain vector of the plastic strain increments, and

$$\begin{aligned} r_{\underline{\varepsilon}_{n+1}}^k &= -\left(\underline{\varepsilon}_{n+1}^p\right)^k + \underline{\varepsilon}_n^p + \Delta\lambda_{n+1}^k \frac{\partial f_{n+1}^k}{\partial \underline{\sigma}_{n+1}^k} \\ r_{f,n+1}^k &= f_{n+1}^k\left(\underline{\sigma}_{n+1}^k\right) \end{aligned} \tag{22}$$

are the residues that should be minimized. The final converged values of the unknowns $(\underline{\sigma}_{n+1}^k, \Delta\lambda_{n+1}^k)$ for the step *n*+1 are obtained through the successive summation of the increments determined at each iteration from the linear system of eqs. (20):

$$\begin{aligned} \underline{\sigma}_{n+1}^k &= \underline{\sigma}_n + \sum_{i=1}^k d\underline{\sigma}_{n+1}^i \\ \Delta\lambda_{n+1}^k &= \sum_{i=1}^k d\lambda_{n+1}^i \end{aligned} \tag{23}$$

Since the second order derivatives of the yield function are quite straightforward, but too long, they are not included in this work for the sake of clarity. The consistent tangent elasto-plastic constitutive matrix can be easily obtained following the procedures described in [9] resulting:

$$d\underline{\sigma}_{n+1} = \left(\underline{H} - \frac{\underline{H}\dfrac{\partial f_{n+1}}{\partial \underline{\sigma}_{n+1}} \dfrac{\partial f_{n+1}}{\partial \underline{\sigma}_{n+1}} \underline{H}}{h + \dfrac{\partial f_{n+1}}{\partial \underline{\sigma}_{n+1}} \underline{H} \dfrac{\partial f_{n+1}}{\partial \underline{\sigma}_{n+1}}} \right) d\underline{\varepsilon}_{n+1} \tag{24}$$

where

$$\underline{H} = \left(\underline{D}_s^{-1} - \Delta\lambda_{n+1} \frac{\partial^2 f_{n+1}}{\partial \left(\underline{\sigma}_{n+1} \right)^2} \right)^{-1} \tag{25}$$

and h is the strain hardening parameter, assumed null in the present study. For the numerical simulations, the values of the parameters included in Table 2 were adopted.

E_s (MPa)	ν_s (-)	γ_s (kN/m^3)	c (kPa)	ϕ ($^\circ$)
20.0	0.3	18.0	5.0	30.0

Table 2 – Values of the properties for the Mohr-Coulomb soil constitutive model.

2.4. Constitutive model for the soil-concrete interface

To simulate the soil - box-culvert interaction, a six-node 2D line interface element was used, which formulation is described elsewhere [5]. The constitutive model of the interface element is simulated with the following relationship:

$$\underline{\sigma}' = \begin{bmatrix} \tau \\ \sigma \end{bmatrix} = \begin{bmatrix} \sigma_1' \\ \sigma_2' \end{bmatrix} = \underline{D}_I \, \Delta\underline{u}' \tag{26}$$

where $\underline{\sigma}'$ is a vector, whose components are the tangential ($\tau = \sigma_1'$) and normal ($\sigma = \sigma_2'$) stress in the local interface coordinate system, $\Delta\underline{u}'$ is a vector of the relative displacements, whose components represent the sliding, s, and the opening, w, of the interface boarders and $\underline{D}_I$ is the constitutive matrix:

$$\underline{D}_I = \begin{bmatrix} D_t & 0 \\ 0 & D_n \end{bmatrix} \tag{27}$$

with D_t and D_n being the tangential and normal stiffness. In the present study it was assumed that no tractions can be transferred between soil and box-culvert, and a linear elastic behaviour occurs when the interface is subject to compression. For modelling the soil-concrete sliding behaviour, the law schematically represented in Fig. 6 was implemented, where:

$$\tau(s) = \begin{cases} \dfrac{\tau_o}{s_o} & if \quad 0 \le |s| \le s_o \\ \tau_m \left(\dfrac{s}{s_m} \right)^{\alpha_1} & if \quad s_o < |s| \le s_m \\ \tau_m \left(\dfrac{s}{s_m} \right)^{-\alpha_2} & if \quad |s| > s_m \end{cases} \tag{28}$$

$$D_t = \begin{cases} \dfrac{\tau_o}{s_o} & if \quad 0 \le |s| \le s_o \\ \alpha_1 \dfrac{\tau_m}{s_m}\left(\dfrac{s}{s_m}\right)^{\alpha_1 - 1} & if \quad s_o < |s| \le s_m \\ -\alpha_2 \dfrac{\tau_m}{s_m}\left(\dfrac{s}{s_m}\right)^{-\alpha_2 - 1} & if \quad |s| > s_m \end{cases} \tag{29}$$

$$\tau_m = \overline{c} - \sigma_n \tan\delta \tag{30}$$

with $\overline{c}$ and δ being the cohesion and the friction angle of the soil-concrete interface, and $\sigma_n = \sigma_2'$ is negative when in compression.

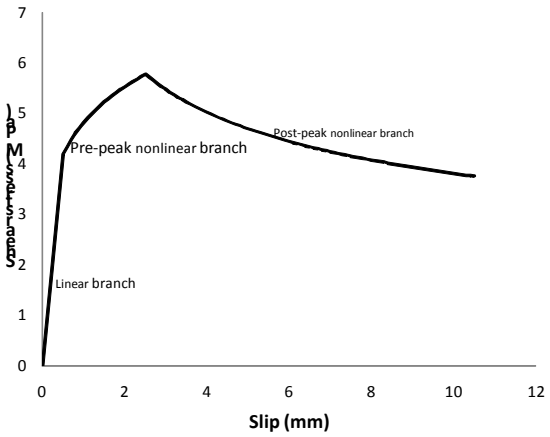

Fig. 6 – Diagram to simulate the soil-concrete sliding behaviour.

For the present study, the values indicated in Table 3 were considered.

s_o (mm)	s_m (mm)	α_1 (-)	α_2 (-)	$\overline{c}$ (kPa)	δ (°)	D_n (kN/m)
0.5	2.5	0.2	0.3	5.0	30.0	1.0e+05

Table 3 – Values of the properties to simulate the soil-concrete sliding behaviour.

2.5. Construction phases and finite element meshes

The simulation of the construction phases was implemented into FEMIX, being possible to have in distinct phases finite elements of different type and constitutive models, as well as distinct support conditions and load cases. For the present study the phases and the corresponding finite element meshes are represented in Fig. 7. The soil and the box-culvert were discretized by 8-noded finite elements, with a 2×2 Gauss-Legendre

integration scheme, while soil-concrete interface was simulated by 6-noded interface elements with a 2 Gauss integration rule. In the analysis, a force convergence criterion with a tolerance of 0.001 was used with a Newton-Raphson technique based on the evaluation of the stiffness matrix in every iteration.

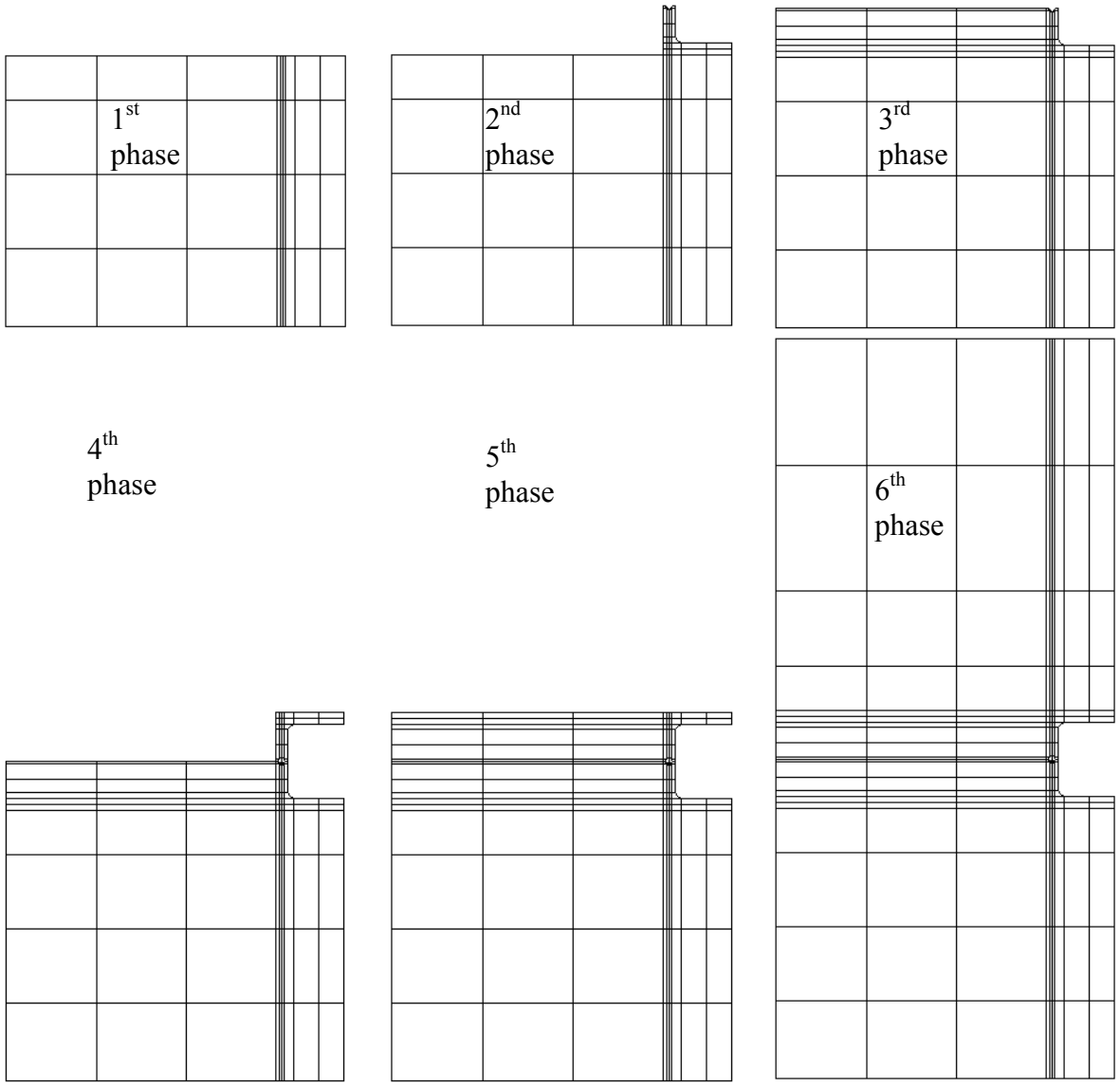

Fig. 7 – Finite element meshes of the sixth construction phases of the present study.

2.6. Load cases

In each phase the self-weigh of the intervening materials (not affected by any factor) is the load case. In the last phase, after having been applied the self-weight of the soil mobilized

in this phase, an edge load applied on the surface of the embankment was increased monotonically in order to simulate a live load up to the attainment of a maximum crack width on the box-culvert of about 0.3 mm (Fig. 2).

3. RESULTS

Due to the limit of space, only the results corresponding to the occurrence of a maximum crack width of 0.27mm are presented. This crack width was estimated multiplying the maximum normal crack strain by the corresponding crack band width. This crack width occurred for a live load (LL, see Fig. 2) of 30 kPa. Fig. 8 represents the displacement fields, while Fig. 9 shows the undeformed and the deformed meshes (for an amplifier factor of the displacements of 11).

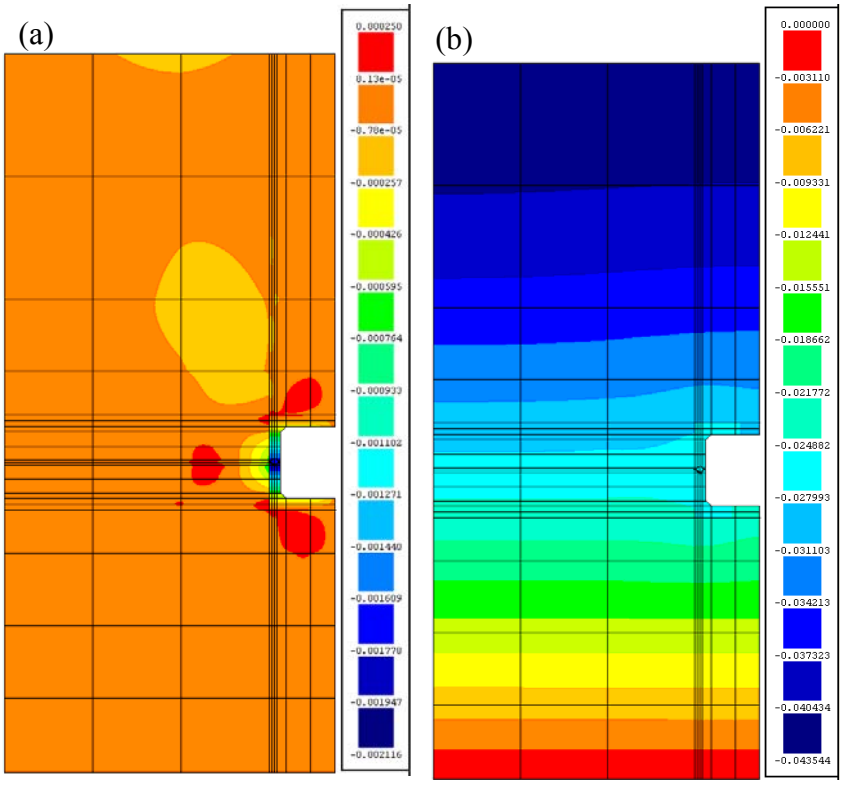

Fig. 8 – Displacement field in *y* (a) and *z* (b) direction (m)

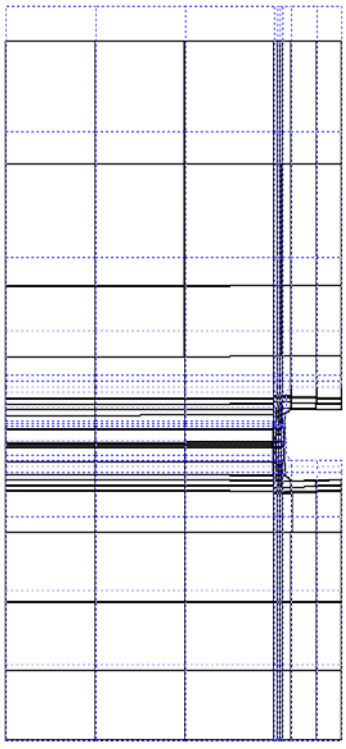

Fig. 9 – Deformed mesh.

The crack pattern is illustrated in Fig. 10, showing that only flexural cracks formed on the top and bottom slabs of the two components composing the box-culvert. As Fig. 11 reveals, in the concrete in contact with the soil, at the symmetry axis of the problem, the σ_y compression stresses attained a maximum value of about 14 MPa, which is, however, lower than the design value of the compressive strength of the SFRSCC considered for the box-culvert. In terms of σ_z stress field, the maximum tensile stresses attained a value of

about 1 MPa in the exterior-top part of the arms of the two components of the box-culvert, near the connection to the slab. The maximum compressive stresses occurred in the hinge connection, but the maximum value is limited to 4.6 MPa. It is also notable that no cracks formed in the hinge region, revealing that the connection was well designed.

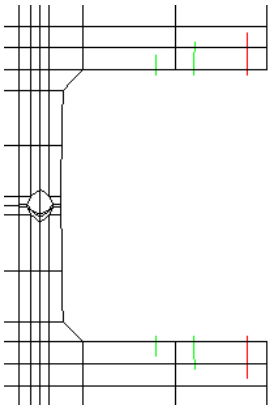

Fig 10 – Crack pattern.

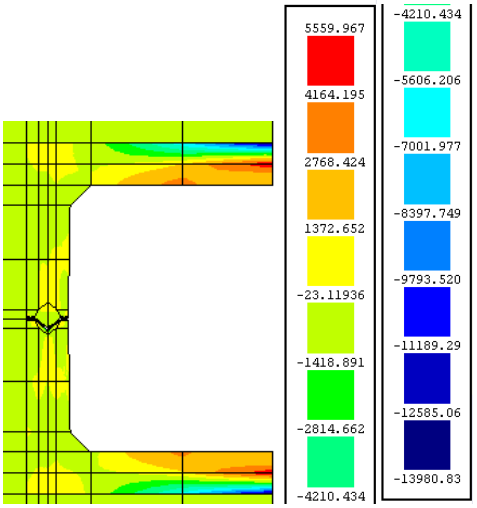

Fig. 11 – σ_y field in the box-culvert (kPa).

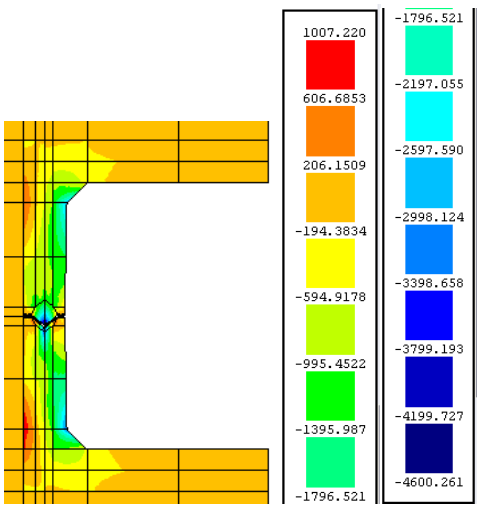

Fig. 12 – σ_z field in the box-culvert (kPa).

The shear stress field in the box-culvert is represented in Fig. 13. The maximum τ_{yz} at the integration points in the shear critical zones is 650 kPa. According to the formulation proposed by RILEM TC 162-TDF committee [10], the shear resistance of a concrete element reinforced with steel stirrups, steel fibres and ordinary longitudinal reinforcement is given by:

$$V_{Rd3} = V_{cd} + V_{fd} + V_{wd} \tag{31}$$

where V_{cd} and V_{wd} represent the contribution of concrete and steel stirrups, respectively, for the shear resistance, determined according to the CEB-FIP Model Code [11], and V_{fd} is the contribution of fibre reinforcement:

$$V_{fd} = 0.7\, k_f\, k_l\, \tau_{fd}\, b_w\, d \ \text{[N]} \tag{32}$$

where k_f and k_l are factors that for the cross sections of the box-culvert assume a unitary value, b_w and d are the width and the depth of the cross section, and,

$$\tau_{fd} = 0.12\, f_{eqk,3} \ [\text{N/mm}^2] \tag{33}$$

where $f_{eqk,3}$ is the characteristic value of the equivalent flexural tensile strength parameter determined under the recommendations of RILEM TC 162-TDF. According to this formulation, if only fibres are used for the reinforcement of the box-culvert the $f_{eqk,3}$ needs

to be higher than 7.7MPa ($V_{fd}/(b_w\, d) = 0.7\,\tau_{fd} = 0.7 \times 0.12\, f_{eqk,3} \geq$ 650kPa, in case of assuming the maximum shear stress as the average one in the shear critical zone). This value is higher than the values registered experimentally for the developed cost competitive SFRSCC for this type of applications. Therefore, it is recommended to apply the minimum percentage of longitudinal conventional reinforcement (according to EC2 of 2002 [12] $A_{s,min}$=0.0003 m^2/m, ρ_{sl}=0.23%, which corresponds to 6ϕ8/m, and 5.1 kg/m^3 of steel) as represented in Fig. 14, since for this percentage $\tau_{cd} = V_{cd}/(b_w\, d)$=503 kPa, which requires a $f_{eqk,3}$ of about 1.75MPa, which is a value that the developed SFRSCC exceeds.

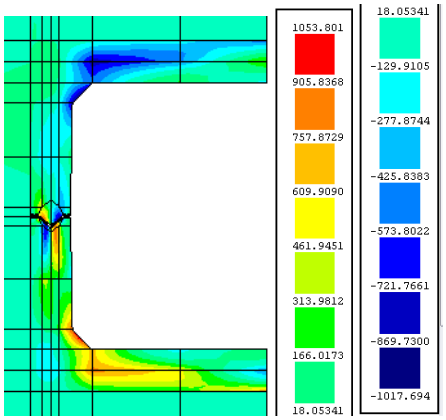

Fig. 13 – τ_{yz} field in the box-culvert (kPa).

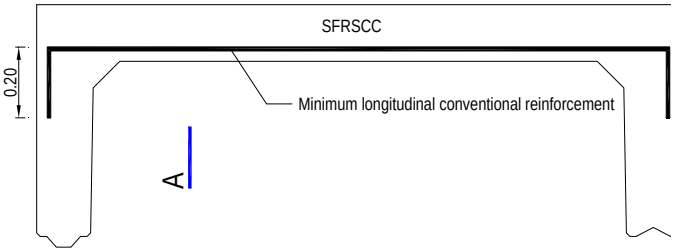

Fig. 14 – Proposed reinforcement.

4. CONCLUSIONS

In this paper a numerical model was briefly described to explore the possibilities of using fibre reinforced concrete for the partial or total replacement of conventional reinforcement in box-culvert underground structures. This is the first part of this research project, therefore some simplifications were adopted mainly for modelling the soil behaviour. In fact, the soil was model by an associated flow rule, elasto-plasticity Mohr-Coulomb yield criterion without any type of hardening. The box-culvert was simulated by a smeared 2D crack model and an interface model based on the Mohr-Coulomb principles and able of simulating a null tensile stress transfer between soil and concrete was developed. The simulation of phase construction process and the new constitutive laws were implemented into FEMIX computer program. A small and very stiff box-culvert was used in the present study, having been concluded that the 118.5 kg/m^3 of reinforcement currently used in this type of box-culvert can be reduced to 5.1 kg/m^3 if the steel fibre reinforced self compacting concrete, already developed within the ambit of another research project, is used. To improve the numerical model, the next research steps are composed by the introduction of a hardening/softening law for the cohesion and friction angle of the soil, the implementation of a non-associated flow rule elasto-plasticity approach in order to better simulate the inelastic soil volume changes, a constitutive law for the mode I

component of the interface, able of simulating the use of appropriate materials at the soil-box-culvert interface in order to promote an oriented stress redistribution and, therefore, minimize the principal tensile stresses in the box-culvert.

7. AKNOWLEDGEMENTS

The first Author wish to acknowledge the support provided by FCT by means of the SFRH/BSAB/818/2008 sabbatical grant, as well as the excellent work conditions provided by Prof. Marco di Prisco. Thanks for the friendship environment of the colleagues of the Lecco Regional Polo of Politecnico di Milano.

REFERENCES

[1] Barros, J.A.O., "Steel fiber reinforced self-compacting concrete – from the material characterization to the structural analysis", HAC2008, 1st Spanish Congress on Self-Compacting Concrete, Valencia, Spain, 31-58, 18-19 February, (2008). /Invited Keynote Lecturer/

[2] Sena-Cruz, J.M.; Barros, J.A.O.; Azevedo, A.F.M.; Ventura Gouveia, A.V. "Numerical simulation of the nonlinear behavior of RC beams strengthened with NSM CFRP strips", CMNE 2007 - Congress on Numerical Methods in Engineering and XXVIII CILAMCE - Iberian Latin American Congress on Computational Methods in Engineering, Abstract pp. 289, Paper nº 485 published in CD – FEUP, 20 pp., Porto, 13-15 June (2007).

[3] Rots, J.G., "Computational modeling of concrete fracture", Dissertation, Delft University of Technology, (1988).

[4] Barros, J.A.O.; Gettu, R.; Barragan, B.E., "Material Nonlinear analysis of Steel fibre reinforced concrete beams failing in shear", 6th International RILEM Symposium on fibre reinforced concrete - BEFIB 2004, Edts. M. di Prisco, R. Felicetti, G.A. Plizarri, Vol. 1, p. 711-720, 20-22 September (2004).

[5] Sena-Cruz, J.M. "Strengthening of concrete structures with near-surface mounted CFRP laminate strips." *PhD Thesis*, Department of Civil Engineering, University of Minho, (2004).

[6] Barros, J.A.O., 'Behaviour of fibre reinforced concrete - experimental and numerical analysis', PhD Thesis, Civil Eng. Dept., FEUP, Portugal, (1995) (in Portuguese).

[7] Pereira, E.B.; Barros, J.A.O., Camões, A.F.F.L., "Steel fiber reinforced self-compacting concrete – experimental research and numerical simulation", Journal of Structural Engineering, 134(8), 1310-1321, August (2008).

[8] Chen, W.F.; Han, D.J., "Plasticity for Structural Engineers", Springer-Verlag, (1988).

[9] Hofstetter, F.; Mang, H.A., "Computational mechanics of reinforced concrete structures", Vieweg, (1995).

[10] RILEM TC 162-TDF, 'Test and design methods for steel fibre reinforced concrete - σ - ε design method - Final Recommendation', Materials and Structures, Vol.36, October (2003), pp. 560-567.

[11] CEB-FIP Model Code, Comite Euro-International du Beton, Bulletin d'Information nº 213/214 (1993).

[12] *prEN 1992-1-1*, Eurocode 2: Design of concrete structures – Part 1: General rules and rules for buildings, April (2002).